Water Practice & Technology

IWA PUBLISHING

Water Practice & Technology Vol 18 No 10, 2384 doi: 10.2166/wpt.2023.154

Valorization of lignocellulosic solid waste obtained from essential oil industry for bio-oil production and dye removal

Sourodipto Modak, Priyanka Katiyar*, Sanjeev Yadav and Annapurna Hans

Department of Chemical Engineering, Shiv Nadar Institution of Eminence (Deemed to be University), Greater Noida 201314, Uttar Pradesh, India
*Corresponding author. E-mail: priyanka@snu.edu.in

PK, 0000-0002-0465-9860

ABSTRACT

This research underscores the potential of utilizing carrot seed waste and its derived biochar as effective solutions for waste management and wastewater treatment applications. This waste is thoroughly characterized for its chemical, thermal, and morphological properties. It is found to be rich in carbon and cellulose, proved suitable for pyrolysis, yielding 25% biochar and 45% bio-oil, with the latter containing carboxylic acids and hydrocarbons. Biochar, characterized by a high surface area of around 300 m^2/g, micro- and mesopores, and the presence of metal oxides, demonstrated outstanding adsorption properties. Biochar shows superior performance compared to raw carrot seed waste, mainly in the context of methylene blue dye removal, obtaining an impressive removal efficiency of 99%. Subsequently, optimization of pH, adsorbent dosage, dye concentration, and reaction temperature is carried out using biochar as the adsorbent to maximize dye removal and adsorption capacity, whereas adsorption kinetics follows pseudo-first-order kinetics.

Key words: adsorption, biochar, characterization, pyrolysis, spent carrot seed

HIGHLIGHTS

- Pyrolysis of carrot seed waste produces 45 wt% bio-oil.
- Carrot seed bio-oil contains caboxylic acids and aliphatic hydrocarbons.
- The porous structure and surface area of biochar are enhanced in comparison with raw waste.
- Biochar turned out to be an excellent adsorbent for dye removal.

GRAPHICAL ABSTRACT

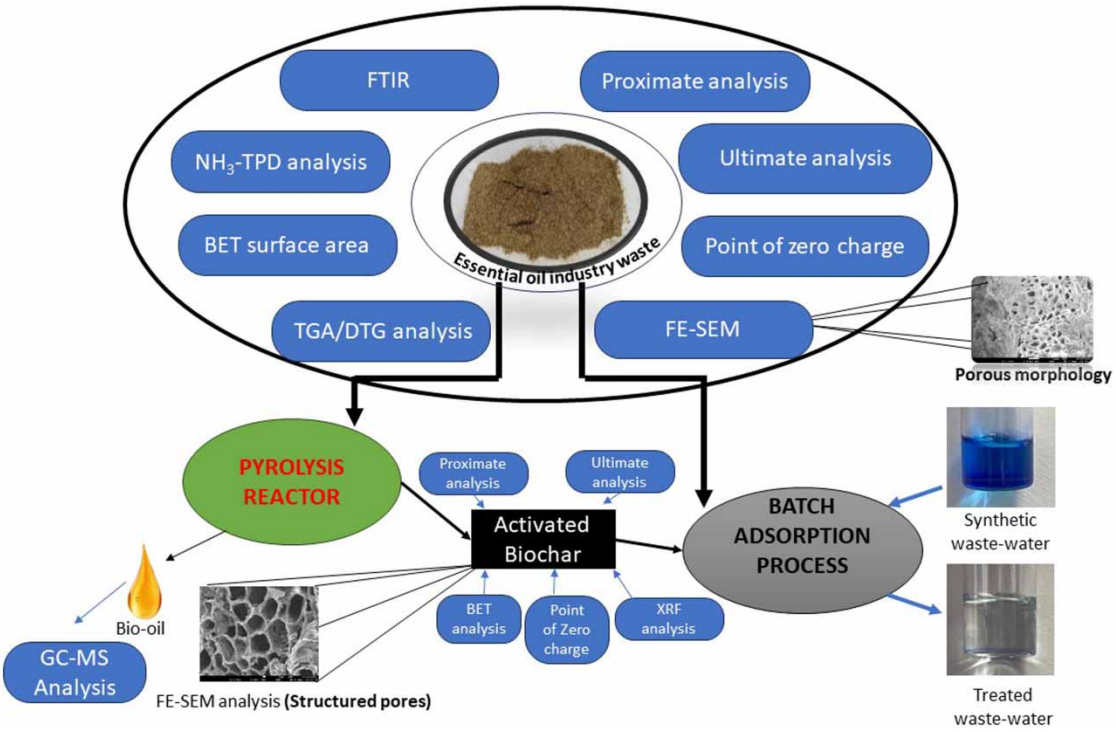

1. INTRODUCTION

Essential oils are vital components of life, renowned for their remarkable medicinal properties, including their ability to induce sleep and alleviate stress and anxiety through aromatherapy. After the extraction of essential oils from natural sources such as ginger, turmeric, pepper, fennel seed, and carrots, the residual solid materials are often disposed of in landfills or incinerated, resulting in environmental pollution (Sowbhagya 2019). It is anticipated that the market for extracted essential oils would expand at a CAGR of 7.4% between 2018 and 2028, resulting in a greater quantity of solid waste (Get News 2022). Consequently, there is an urgent need to explore methods for the value-added utilization of these spent solid residues to ensure both economic and environmental sustainability.

It is noteworthy that various spent solid wastes from the essential oil industry have been the subject of research for extracting value-added compounds, serving as adsorbents, and even for biofuel production (Kumar & Ahmad 2011; Alismaeel *et al.* 2022). However, no study has reported the complete valorization of carrot seed waste. A recent report has indicated that the market for carrot seed oil is expected to experience robust growth by 2029 owing to its popularity in aromatherapy and antimicrobial, antioxidant, and antifungal characteristics, especially in North America, Latin America, Europe, East Asia, South Asia, Oceania and Middle East, and Africa (Sieniawska *et al.* 2016). Carrot seeds contain only 10–15 wt% of essential oils resulting in around 85–90 wt% of carrot seed as the solid waste which requires proper disposal and management. Carrot seed waste can be utilized by two ways: (i) feedstock for bio-oil production and (ii) as an adsorbent (raw and biochar) for wastewater treatment. It is a suitable candidate for bio-oil production through slow pyrolysis due to its high lignocellulosic content that produces bio-oil, biochar, and little amount of syn gas (Yin *et al.* 2021). Bio-oil has versatile applications, including biodiesel and chemical production, while biochar is predominantly utilized for remediating contaminants in soil, water, and air due to its ample surface area, high porosity, functional groups, cation exchange capacity, and stability (Wang *et al.* 2023).

Nowadays, most textile industries are responsible for creating water pollution by discharging untreated dye-bearing effluent streams into water bodies. Methylene Blue (MB) dye is a commonly used dye in the textile industry that could be highly toxic to human health, causing tissue necrosis, vomiting, nausea metal, neural disorder, and methemoglobinemia (Abu-Dief *et al.* 2021b; Alahmadi *et al.* 2023). Several treatment processes (conventional and advanced), such as coagulation–flocculation, biological treatment, adsorption, oxidation, have been

studied to treat dye-bearing wastewater (Mohamed & Abu-Dief 2018; Mohsen Alardhi *et al.* 2020; Ali *et al.* 2022b; Alzaid *et al.* 2023). Among all, biosorbent-based adsorption has garnered particular interest due to its effectiveness and eco-friendliness (Al-Jaaf *et al.* 2022). Agro-industrial waste, due to its affordability, widespread availability, and ease of use, presents favorable characteristics such as porous morphology, crystalline nature, and metal oxide content for effective adsorption applications (Al-Jaaf *et al.* 2022).

The primary objective of this study is to repurpose spent carrot seed waste (SCSW) for dual applications: (i) bio-oil production and (ii) the treatment of MB-containing wastewater. Initially, a comprehensive characterization of SCSW is carried out using techniques such as field emission-scanning electron microscopy (FE-SEM), Brunauer-Emmett-Teller (BET), proximate analysis, thermogravimetric analysis (TGA), and differential thermal analysis (DTG), Fourier transform infrared (FTIR), and ammonia-temperature programmed desorption (NH_3-TPD). Subsequently, SCSW undergoes pyrolysis at 500 °C in a fixed bed reactor to yield bio-oil and biochar. Additionally, the GC-MS analysis of the bio-oil is carried out to identify its composition and constituent compounds. Finally, to assess the efficacy of SCSW and its biochar as adsorbents, a batch adsorption study is performed for the removal of MB from wastewater. It is worth noting that this study represents a novel, comprehensive examination of the value-added utilization of SCSW, as no prior research has explored all these aspects simultaneously.

2. MATERIALS AND METHODS

All the chemicals used in the present work were of analytical reagent (AR) grade. The MB powder (Q39692) and NaOH (97% purity) are procured from Thermo-Fisher Scientific; HCl (35%) is purchased from Rankem; KOH (86%) and chloroform (99.9%) are procured from Agnitio pharma. Orbital Shaking Incubator, UV-spectroscopy, and pH meter are procured from Labgear International, Labtronics (LT-2204) and Metrex auto deluxe, India, respectively. Double-distilled water is used throughout the analysis. The SCSW sample is procured from Rajeshwari Essential Oil Company, located in India and washed repeatedly with de-ionized (DI) water using a G2 funnel until a clear supernatant is achieved and then subjected to a drying process in a vacuum air oven at 80 °C, for a duration of 24 h to eliminate moisture. The dried SCSW sample was subsequently stored in an airtight container for further research.

2.1. Characterization of SCSW

Proximate analysis of SCSW is carried out by adopting the method as per the ASTM D 121 method (Singh & Yadav 2019) and elemental analysis is carried out in Thermo Finnigan Flash 1112 Series Elemental analyzer. The fixed carbon content of the SCSW sample is calculated using the following equation:

$$\text{Fixed carbon (\%)} = 100 - (\%\text{water content} + \%\text{volatile matter} + \%\text{ash}) \quad (1)$$

BET surface area analysis is conducted using Autosorb 1 (Quanta chrome) with nitrogen gas to analyze adsorption–desorption isotherm at 77.35 K. The pH drift method is used for point-of-zero charge determination (Gadelha *et al.* 2023). In this method, 50 mL of 0.01 M NaCl is added to 10 conical flasks with pH adjusted from 3 to 12 using 0.1 M HCl and 0.1 M NaOH. Subsequently, 0.15 g of the SCSW sample is added to each conical flask, which is then sealed and placed in an orbital shaking incubator for 48 h at 30 °C to reach equilibrium. After 48 h, the filtrate is collected from each conical flask, and pH_{final} is measured using a pH meter. The graph is plotted between ΔpH ($pH_{final} - pH_{initial}$) vs. $pH_{initial}$ to find the intersection point where $\Delta pH = 0$ gives the pH_{pzc} of SCSW. The experiments are conducted in triplicates.

TPD analysis is carried out using Micrometrics Auto ChemII 2750 instrument. For this, 50 mg of the SCSW sample is loaded into a U-shaped quartz reactor and preheated at 200 °C for 2 h in the He atmosphere (20 mL/min). After cooling to room temperature, the sample is exposed to 10% ammonia in the He environment and heated at 10 °C/min for 60 min till adequate ammonia is adsorbed onto the SCSW surface. In the final step, the SCSW sample is heated in helium environment from 50 to 950 °C at a rate of 20 °C/ min for 90 min to obtain thermal conductivity detector (TCD) signals.

For FE-SEM analysis (JOEL7610F), SCSW samples are gold-coated prior to capture images at 900× and 1,500× magnification levels. FTIR analysis is performed using Nicolet iS20 FTIR Spectrometer (Thermo Scientific), where 10 mg of the sample is taken in ATR crystal, clamped using a pressure gauge, and placed in the FTIR instrument sample holder. The IR scanning is done from 500 to 4,000 cm^{-1} range with a 1 cm^{-1} gap and the scanning time is 20 s. TGA/DTG analysis is carried out using Thermogravimetric Analyzer (Mettler Toledo). Nine mg

of the SCSW sample is isothermally held at 35 °C for 5 min, and then heated to 800 °C at a rate of 10°C/min. Nitrogen gas flows at a constant rate of 40 mL/min throughout the analysis.

2.1.1. Pyrolysis of SCSW

Pyrolysis of SCSW is carried out using a thermochemical conversion setup, consisting of a fixed bed reactor (34 mm dia. and 410 mm height) housed within a furnace, as presented in Supplementary material, Figure S1. The reactor is insulated with glass wool, and the temperature of the heater is controlled using a proportional integral -derivative (PID) controller. An inert atmosphere is maintained using nitrogen with a flow rate of 100 mL/min. Fifty g of SCSW is fed to the reactor and heated to 500 °C with a rate of 10 °C/min for 60 min. In downstream of the setup, a condenser is deployed alongside a liquid–gas separator for the collection of the resulting bio-oil. Percentage gas yield is estimated by deducting the weight of bio-oil and biochar from the original feed mass (Kumari & Mohanty 2020). To identify the chemical compounds in bio-oil, GC-MS (Agilent 5977B GC/MSD) is used with HP-5MS capillary column (30m × 0.25 mm, 0.25 μm). The bio-oil sample is prepared by diluting with chloroform (HPLC-grade) in the ratio of 1:10 and then injected at a split ratio of 1:10. The initial temperature of the column is kept at 60 °C, and then the temperature is raised to 300 °C at a ramping rate of 2 °C/min. Helium is used as a carrier gas with a flow rate of 3 mL/min, and the compounds are identified using NIST library.

2.1.2. Activation of biochar

Biochar derived from the pyrolysis of SCSW is activated by following the procedure given by dos Santos *et al.* (2019). Ten g of SCSW biochar is taken in a 250-mL round bottom flask with 100 mL of 8 M KOH and connected to a reflux condenser. The mixture is heated in an oil bath at 80 °C for 2 h at 120 rpm and filtered, and then biochar is kept in an air oven for 12 h at 110 °C. Further thermal treatment of activated biochar (ABC) is done by heating the sample in the tubular furnace at a controlled heating rate of 10 °C/min to achieve the final temperature of 800 °C for 90 min. The sample is then cooled and washed several times with distilled water until the final pH of supernatant reaches 7. After washing, samples are kept in an air oven at 110 °C for 12 h.

2.1.3. Adsorption study

A stock solution with a concentration of 1,000 ppm of MB is prepared by dissolving 1,000 mg of MB in 1,000 mL of deionized (DI) water in a volumetric flask. A 100-ppm working standard solution of MB is prepared from stock solution which is subsequently diluted to obtain solutions ranging from 0 to 10 ppm, each with a volume of 10 mL. The absorbance values of these MB solutions with a wavelength of $\lambda_{max} = 665$ nm are recorded using a UV spectrophotometer. Then, a calibration curve is plotted to get a correlation between absorbance and concentration that is given in Supplementary material, Figure S2. For batch adsorption experiments, 100 mL of MB dye solution is taken into a 150-mL conical flask with the desired amount of SCSW/ABC and placed in an orbital shaking incubator. The natural pH of the dye solution is only considered for the experiment. The concentration of the dye solution is determined by measuring its absorbance both before and after the adsorption run using UV spectroscopy. Subsequently, the concentration is calculated using the calibration curve equation. The experiments are carried out in triplicate to ensure the proper validation of the results. The adsorption capacity and removal efficiency are calculated using Equations (2) and (3) (Abdel-Rahman *et al.* 2016; Abu-Dief *et al.* 2021a):

$$q_e = \frac{(C_0 - C_e) \times \mathrm{V}}{W} \tag{2}$$

$$\%\ \text{Dye removal} = \frac{C_0 - C_f}{C_0} \times\ 100 \tag{3}$$

where C_0, C_e, and C_f are initial, equilibrium, and final dye concentration (mg/L), respectively, q_e is adsorption capacity (mg/g), W is adsorbent mass (g), V is the volume of dye solution (ml)

3. RESULTS AND DISCUSSIONS

3.1. Characterization of SCSW

3.1.1. Proximate and ultimate analyses

From the ultimate analysis given in Table 1, the presence of high carbon content can be seen due to the organic attributes of SCSW. The carbon-containing lignocellulose could be helpful for the adsorption of organic

Table 1 | Physio-chemical characterization and surface area analysis of SCSW and ABC

Ultimate analysis of SCSW											
Component	Carbon (%)	Hydrogen (%)	Oxygen (%)	Nitrogen (%)	Sulfur (%)						
Weight%	39.2	5.87	39.02	3.69	0.48						
Proximate analysis of SCSW											
Component	Moisture (%)	Volatile Matter (%)	Ash (%)	Fixed carbon (%)	HHV (MJ/kg)						
Weight%	6.9	71.3	13.3	8.5	14.02						
BET surface area, pore volume, diameter, and acidic sites of SCSW											
BET surface area (m^2/g)	2.6										
BJH adsorption cumulative volume of pores (cm^3/g)	0.002										
BJH desorption average pore diameter (Å)	27										
Acidic sites (μmol/g)	96										
Ultimate analysis of ABC											
Component	Carbon (%)	Hydrogen (%)	Oxygen (%)	Nitrogen (%)	Sulfur (%)						
Weight%	40.8	1.95	21.9	2.56	0.05						
Proximate analysis of ABC											
Component	Moisture (%)	Volatile Matter (%)	Ash (%)	Fixed Carbon (%)	HHV (MJ/kg)						
Weight%	1.0	27.1	41.4	30.4	14.67						
XRF analysis of ABC											
Oxides	Na_2O	MgO	Fe_2O_3	SiO_2	P_2O_5	SO_3	K_2O	CaO	Al_2O_3	TiO_2	MnO
Weight%	12.1	4.2	5.3	14.6	7.1	7.3	7.9	29.0	3.5	0.28	0.28
BET surface area, pore volume and diameter of ABC											
BET surface area (m^2/g)	300.1										
BJH adsorption cumulative volume of pores (cm^3/g)	0.237										
BJH desorption average pore diameter (Å)	31.67										

compounds or heavy metals from the wastewater (Wang *et al.* 2023). H/C and O/C ratios are 1.7 and 0.75, respectively, which fall within the range of typical lignocellulosic biomass as per the Van Krevelen diagram. Nitrogen content is less, thus, low amount of nitrogen oxides will be produced during the thermochemical conversion process (Saikia & Bardalai 2018). The proximate analysis (Table 1) shows that the ash content is comparatively more than fixed carbon content due to the presence of metals and inorganic compounds, making SCSW different from typical lignocellulosic biomass. The presence of high volatile content (71.3%) in SCSW is comparable to other conventional lignocellulosic biomass, such as brewer's spent gram, having a volatile content of 74% (Saikia & Bardalai 2018). Biomass with higher volatile matter is considered suitable for pyrolysis due to high reactivity and better de-volatilization that lead to the release of gases such as methane, hydrogen, carbon monoxide, and carbon dioxide (Saikia & Bardalai 2018).

3.1.2. BET, TPD, and pH_{pzc} analysis of SCSW

The BET N_2 adsorption–desorption isotherm of SCSW, shown in Figure 1(a), represents the Type IV isotherm with Type H_2(b) hysteresis loop, indicating that SCSW contains a mixture of micro-and mesopores (Cychosz & Thommes 2018). Here, simultaneous multilayer adsorption and capillary condensation of N_2 are taking place with an increase in relative pressure. The BET surface area, shown in Table 1, is found to be less (2.6 m^2/g) in comparison with activated carbon (>60 m^2/g) which is expected in the case of untreated natural biomass. However, it surpasses the surface area of other lignocellulosic adsorbents such as pinecone shells and date seed powder, which exhibit surface areas of 0.64 and 1.2 m^2/g, respectively (Almendros *et al.* 2015; Ali *et al.* 2022a). As illustrated in the pore size distribution plot given in Figure 1(a), the predominant pore

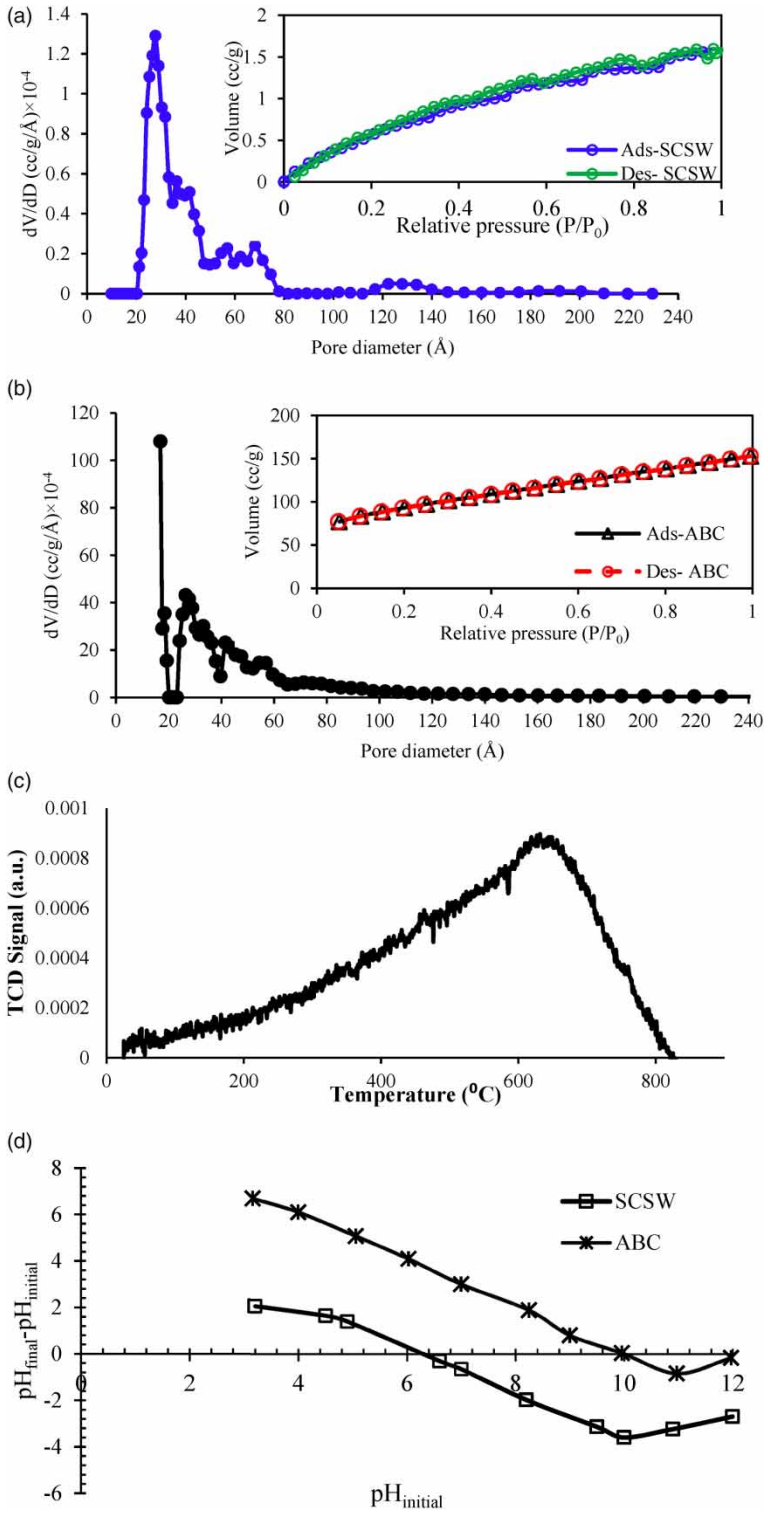

Figure 1 | BET isotherm and pore size distribution plots: (a) SCSW; (b) ABC; and (c) TPD analysis of SCSW. (d) Point-of-zero charge of SCSW and ABC.

size range within the SCSW falls between 20 and 50 Å. Furthermore, as indicated by the BET data in Table 1, the SCSW sample exhibits a favorable pore width but comparatively lower pore volume. This observation implies that the adsorption of organic pollutants is likely to occur primarily through surface groups (chemisorption) rather than within the pores themselves (Omorogie *et al.* 2016).

In TPD analysis of SCSW as shown in Figure 1(c), the single desorption peak between 600 and 700 °C represents the strong acidic sites due to acidic functional groups (OH, C = O, or COOH) (Gadelha *et al.* 2023). The concentration of acidic sites is found to be 96 μmol/g which is comparable with the concentration of an aluminum hydroxide fluoride catalyst (94 μmol/g) (Hemmann *et al.* 2014). Since these acidic groups are of high strength, this could facilitate the adsorption of basic dyes onto the surface of SCSW. Further adsorption of basic dye can be explained through pH_{pzc} analysis of SCSW, as shown in Figure 1(d). It depicts that the pH_{pzc} of SCSW is 6.2, which indicates that it has a negatively charged surface above pH 6.2 and positively charged surface below 6.2. Hence, it can be perceived that SCSW will attract positive ions in basic pH range and negative ions in acidic pH range.

3.1.3. FE-SEM analysis of SCSW

The morphology of SCSW, shown in Figure 2(a) and 2(b), indicates the presence of heterogeneous morphology with a honeycomb-like structure where many pores are visible. These pores are conducive to the adsorption of organic matter on to the surface and inside the pores of SCSW. Organic matter can easily penetrate through the ridges and then quickly get lodged on the surface functional groups and active sites inside the pore. Attachment of molecules occurs due to surface interactions between organic pollutant and surface functional groups of SCSW. The surface functional groups on the surface offer the binding sites for organic pollutant to get adsorbed. Similar morphology was found in *Syringa vulgaris* leaves to efficiently adsorb the MB dye (Mosoarca *et al.* 2020).

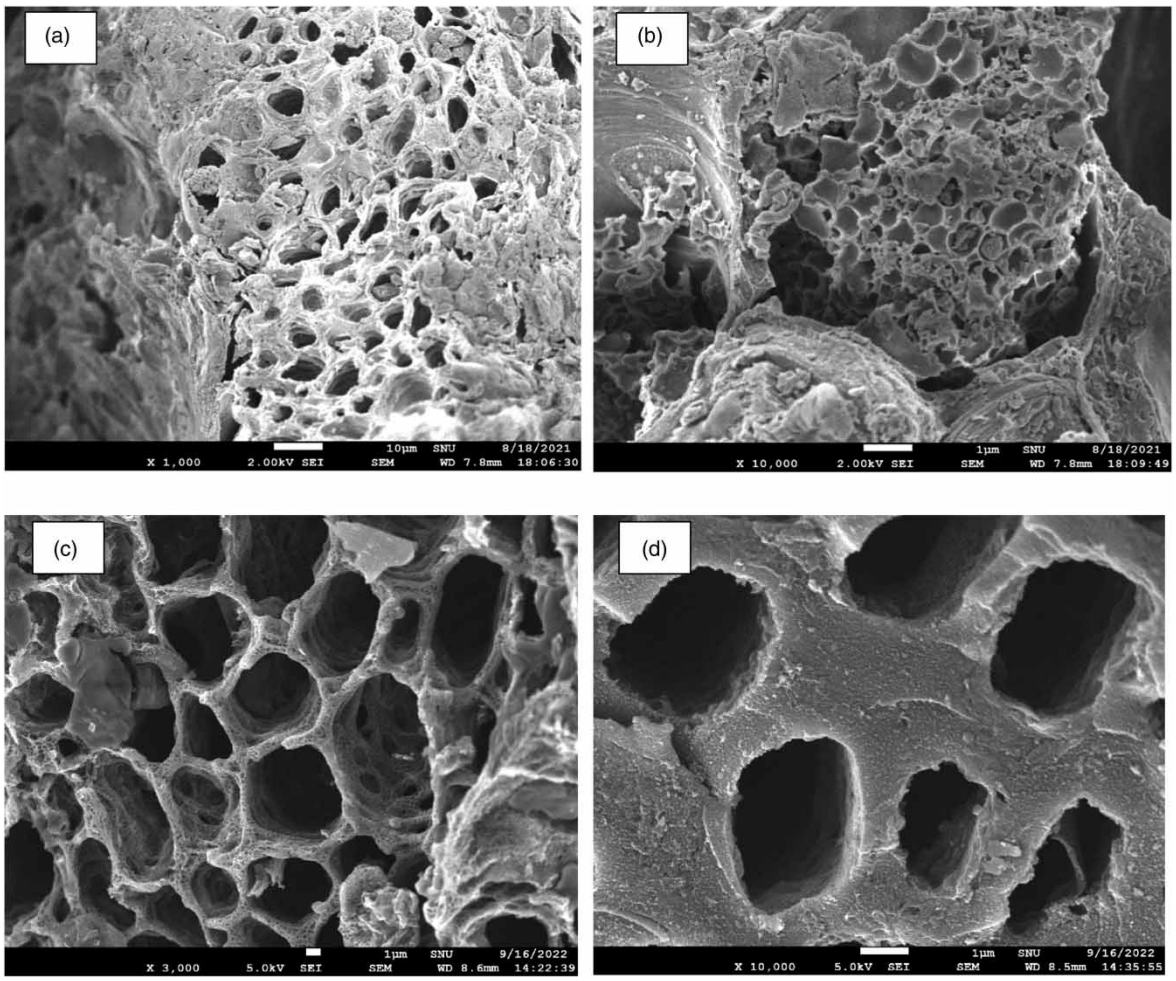

Figure 2 | FE-SEM images: (a) and (b) SCSW and (c) and (d) ABC.

3.1.4. FTIR analysis of SCSW

FTIR spectra of SCSW, given in Figure 3, represent a large hump at 3,320 cm^{-1} corresponding to the hydroxyl group of cellulose, hemicellulose, and lignin (Wakejo *et al.* 2023). The peaks at 2,982^{-} and 2,929 cm^{-1} are

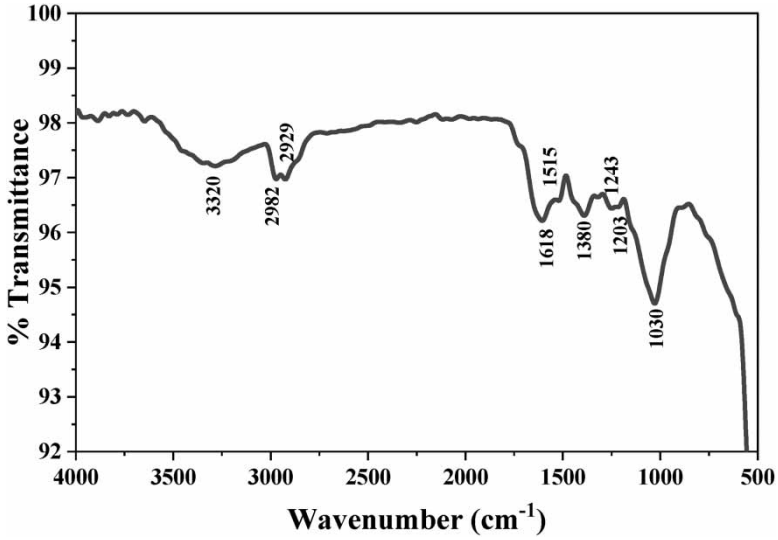

Figure 3 | FTIR spectrum of SCSW.

attributed to C–H–C stretching (asymmetric and symmetric). At 1,618 cm^{-1}, C = O stretching is observed in hemicellulose, lignin, and protein. A peak at 1,515 cm^{-1} reflects the presence of C–N or N–H stretching of amide groups present in the protein bio-polymer (Gadelha *et al.* 2023). The peak at 1,380 cm^{-1} corresponds to C–H bending, which is present in cellulose, hemicellulose, and lignin (Wakejo *et al.* 2023); 1,243 cm^{-1} represents the presence of alkoxy stretches (C–O), and C–O stretch present in lignin, cellulose, and hemicellulose, and 1,203 cm^{-1} shows OH bending of cellulose and hemicellulose (Wakejo *et al.* 2023); 1,030 cm^{-1} shows C–O, C = C, and C–C–O stretch, respectively, present in cellulose, hemicellulose, and lignin (Gadelha *et al.* 2023).

3.1.5. TGA and DTG analysis of SCSW

TGA and DTG plots of SCSW, shown in Figure 4, is divided into three stages of mass loss with the advent of the following temperatures: (i) ambient to 200 °C, (ii) 200–500 °C, and (iii) 500–800 °C. In the first stage, 10% weight loss occurs due to the de-volatilization of lighter hydrocarbons and moisture loss confirmed by a sharp moisture peak at 50 °C in the DTG plot. The second stage corresponds to the significant mass loss of 58% and the DTG peak at 325 °C due to the decomposition of cellulose, hemicellulose, and combustion of carbon species (Saikia & Bardalai 2018). In the third stage, continuous and thermal degradation of lignin or high-molecular-weight components could be seen at a much lower rate due to degradation of heavier volatiles, cracking of C–C bonds, and

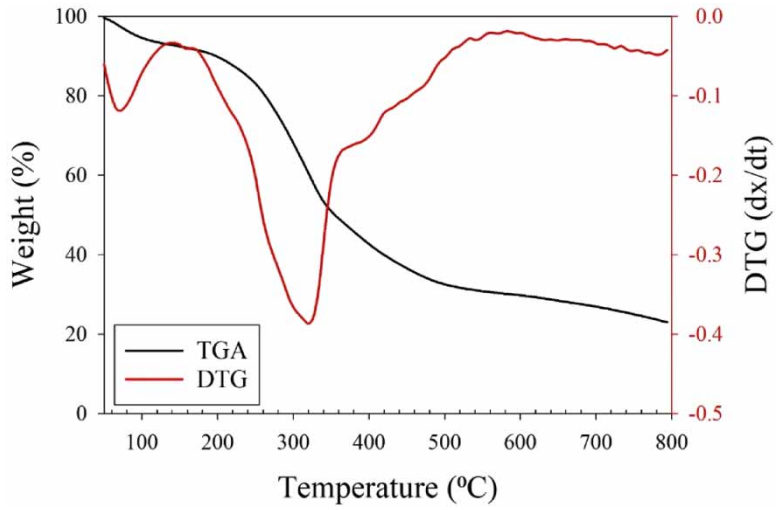

Figure 4 | TGA/DTG analysis of SCSW.

char formation (Saikia & Bardalai 2018). TGA/DTA shows the thermochemical conversion of SCSW will occur at or beyond 500 °C hence pyrolysis was performed at 500 °C.

3.2. Pyrolysis study and bio-oil analysis

As suggested by TGA of SCSW, complete pyrolysis of cellulosic matter takes place at or beyond 500 °C; pyrolysis study was carried out at 500 °C. The pyrolysis of SCSW yielded 45% of bio-oil, 30% pyrolysis gases, and 25% goes into biochar. SCSW bio-oil was analyzed through GC-MS for its qualitative and quantitative analyses. Table 3 represents the total 74 identified compounds present in bio-oil with their retention time and peak area which are further categorized and shown in Figure 5. The GC-MS chromatogram of bio-oil is provided in Supplementary material, Figure S3. As can be seen from Table 2 and Figure 5, bio-oil contains low to heavy hydrocarbons ranging from C_4 to C_{29}. The carboxylic acids are abundant, covering around 35% of total oil, followed by aliphatic hydrocarbon (25%) > oxygenated hydrocarbon > (16%) > alcohols (11%) > aromatic hydrocarbon (6%). Other than these, nitrile, oxane, amine, ketone, and aldehyde compounds are also present in less quantity. The carboxylic acids are responsible for the corrosiveness of bio-oil that can be converted into liquid hydrocarbons using the catalytic cracking process (Wang *et al.* 2012). Aliphatic hydrocarbon and aromatic hydrocarbons indicates the good quality of bio-oil that ensures good combustion properties (Santos *et al.* 2019). Since SCSW bio-oil contains a large amount of carboxylic acids, bio-oil needs to be upgraded using catalytic upgradation techniques before being utilized in liquid transportation infrastructures. Biochar is further activated to enhance its surface properties before using it to treat MB-containing wastewater.

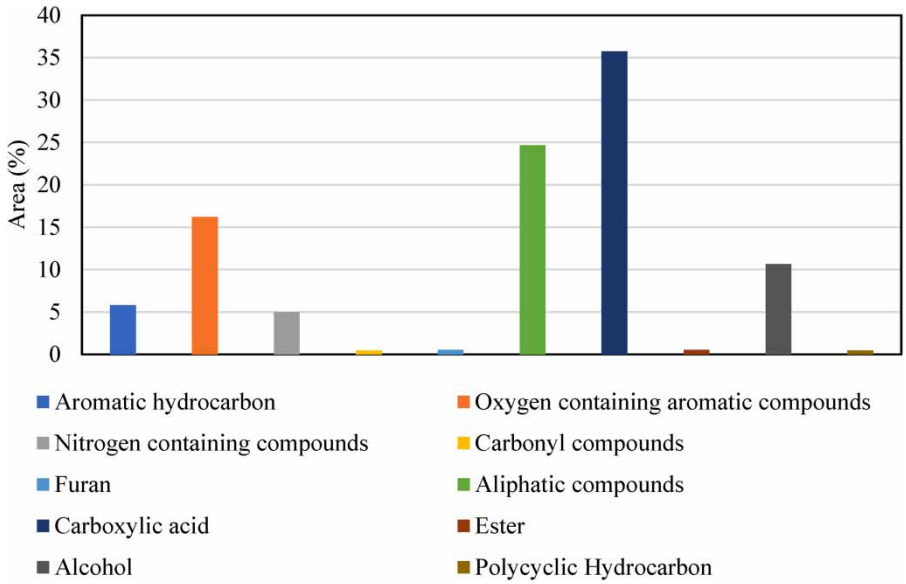

Figure 5 | Fraction of various organic compounds present in SCSW bio-oil.

3.3. Characterization of SCSW-ABC

Biochar has shown encouraging outcomes in the process of removing pollutants from wastewater due to its increased carbon content, surface area, morphological structure, and surface charge (Wakejo *et al.* 2023). To examine the same, ultimate, proximate, BET surface area, SEM, XRF, and point-of-zero charge analysis of ABC are performed and results are tabulated in Table 1. In ultimate analysis of ABC, given in Table 1, H/C and O/C ratios are found to be 0.57 and 0.4, respectively, which lie within the range of char according to the Van Krevelen diagram. Proximate analysis shows that ash and fixed carbon content are increased whereas volatile matter and moisture content are decreased in the carbonization process from SCSW to ABC. It is a result of progressive concentration of minerals and destructive volatilization of ligno-cellulosic matters under high temperature (~500 °C) result. According to XRF results of ABC, given in Table 1, the most prevalent constituents are CaO (29%), SiO_2 (14.6%), and Na_2O (12.1%). Other oxides such as iron, magnesium, and aluminum oxides are

Table 2 | Composition of SCSW bio-oil obtained from pyrolysis of SCSW

Compound name	Formula	Peak area (%)	Compound name	Formula	Peak area (%)
Carboxylic acid			**Alkane**		
Stearic acid	$C_{18}H_{36}O_2$	15.27	Hexadecane	$C_{16}H_{34}$	1.57
14-Pentadecenoic acid	$C_{15}H_{30}O_2$	5.22	Decane	$C_{10}H_{22}$	1.54
Myristic acid	$C_{14}H_{28}O_2$	3.76	Hepadecane	$C_{17}H_{36}$	1.38
Oleic acid	$C_{18}H_{34}O_2$	3.34	Undecane	$C_{11}H_{24}$	1.27
6-Octadecenoic acid	$C_{18}H_{34}O_2$	2.02	Cyclododecane	$C_{12}H_{24}$	0.86
6-Octadecenoic acid	$C_{18}H_{34}O_2$	1.83	Heneicosane	$C_{21}H_{44}$	0.85
Erucic acid	$C_{22}H_{42}O_2$	1.70	Eicosane	$C_{20}H_{42}$	0.54
trans-13-Octadecenoic acid	$C_{18}H_{34}O_2$	1.00	Pentadecane	$C_{15}H_{32}$	0.37
Palmitoleic acid	$C_{16}H_{30}O_2$	0.42	Nonane	$C_{19}H_{20}$	0.37
Hexadecanoic acid	$C_{17}H_{34}O_2$	0.35	Octadecane	$C_{18}H_{38}$	0.36
cis-7-Hexadecenoic acid	$C_{17}H_{32}O_2$	0.32	Undecane	$C_{11}H_{24}$	0.23
cis-Vaccenic acid	$C_{18}H_{34}O_2$	0.30	Octane	C_8H_{18}	0.21
9-Octadecenoic acid	$C_{19}H_{36}O_2$	0.23	**Alkenes**		
Sesquiterpene alcohol			Nonacos-1-ene	$C_{29}H_{58}$	2.37
Carotol	$C_{15}H_{26}O$	5.92	1-Nonadecene	$C_{19}H_{38}$	2.36
Copaene	$C_{15}H_{24}$	0.48	9-Nonadecene	$C_{19}H_{38}$	2.35
β-Santalol	$C_{15}H_{24}O$	0.34	Cetene	$C_{16}H_{32}$	2.32
Nerolindol	$C_{15}H_{26}O$	0.29	Henicos-1-ene	$C_{21}H_{42}$	1.54
Phenols			3-Dodecene,(Z)-	$C_{12}H_{24}$	1.53
2,4-Di-tert-butylphenol	$C_{14}H_{22}O$	4.42	1-Tetracosene	$C_{24}H_{48}$	1.06
Phenol,2,6-bis(1,1-Dimethylethyl)	$C_{15}H_{24}O$	3.91	1-Tetradecene	$C_{14}H_{28}$	0.84
p-Cresol	C_7H_8O	2.40	1-Hexacosene	$C_{26}H_{52}$	0.40
Phenol,2,4-dimethyl	$C_8H_{10}O$	0.66	3-Octene,(Z)-	C_8H_{16}	0.34
Phenol,4-ethyl	$C_8H_{10}O$	0.58	**Aromatic hydrocarbon**		
Phenol,3-methyl	C_7H_8O	0.58	Toluene	C_7H_8	2.33
Phenol,4-ethyl-2-methoxy-	$C_9H_{12}O$	0.42	Indole	C_8H_7N	1.16
2-Methoxy-4-vinylphenol	$C_9H_{10}O_2$	0.32	Styrene	C_8H_8	0.96
cis-Pinen-3-ol	$C_{10}H_{16}O$	0.29	Ethylbenzene	C_8H_{10}	0.80
Phenol	C_6H_6O	2.06	1H-Indole,2-methyl	C_9H_9N	0.77
Alcohol			o-xylene	C_8H_{10}	0.66
1-Hexadecanol	$C_{16}H_{34}O$	2.64	Pyrrole	C_4H_5N	0.54
2,4-Decadien-1-ol	$C_{10}H_{18}O$	1.20	Naphthalene	$C_{10}H_8$	0.49
2-Furan methanol	$C_5H_6O_2$	0.35	p-xylene	C_8H_{10}	0.35
Eucalyptol	$C_{10}H_{18}O$	0.25	Indene	C_9H_8	0.21
Nitrile			Benzofuran,2,3-dihydro	C_8H_8O	0.18
Heptadecanenitrile	$C_{17}H_{33}N$	0.74	**Amine**		
Benzyl nitrile	C_8H_7N	0.34	Amphetamine	$C_9H_{13}N$	0.36
Benzenepropanenitrile	C_9H_9N	0.33	**Ketone**		
Hexenenitrile	C_6H_9N	0.22	2-cyclopenten-1-3-methyl	C_6H_8O	0.24
Oxane			**Aldehyde**		
Daucol	$C_{15}H_{26}O_2$	0.58	2-Dococenal (E)	$C_{10}H_{18}O$	0.24
Other oxygenated group			**Fatty alcohol**		
9-Octadecenamide, (Z)–	$C_{18}H_{35}NO$	0.53	Dodecyl acrylate	$C_{15}H_{18}O_2$	0.52

found in a significant amount as well, with percentages of 5.3, 4.2, and 3.5%, respectively. Table 1 lists the BET surface area, pore volume, and pore diameter of ABC as 300 m^2/g, 0.237 cm^3/g, and 31.67 Å, respectively. It shows that porosity and surface area are greatly enhanced after thermal treatment due to devolatilization at higher pyrolysis temperatures. This leads to an increase in surface area as well as enhanced porous morphology. Both surface area and pore volume are improved by ~115 times compared to SCSW. The adsorption–desorption isotherms of SCSW, given in Figure 1, shows a linear increase in volume adsorbed with the increase in relative pressure that exhibits the type II isotherm where unrestricted mono-multilayer adsorption takes place. Pore size distribution plot of ABC confirms the presence of mainly micropores (≤20 Å) as well as mesopores (20–200 Å) (Das & Debnath 2021).

FE-SEM images of ABC, given in Figures 2(b) and 2(c), represent the honey-comb structure similar to SCSW; however, wider and deeper pores with enhanced porosity and roughness are visible in ABC due to the release of volatile organic matter during the pyrolysis process which is confirmed by BET surface area analysis also. When surface roughness is increased, the surface tends to become more hydrophilic, leading to a reduction in the contact angle between the surface and the interface that typically falls below 90° (Li *et al.* 2021). Another significant factor is the presence of charged groups on the surface of the adsorbing medium which contribute to increased hydrophilicity at the interface between the adsorbate solution and the adsorbent surface (Li *et al.* 2022). In the present work, the NH_3-TPD analysis of SCSW indicates a substantial presence of strong acid sites on the surface that correlates with the existence of strong charged groups. Consequently, the MB dye solution exhibits hydrophilic tendencies toward the surface of the SCSW.

3.4. Adsorption study

The enhancement in adsorption capability of ABC was tested and compared with the raw SCSW sample to adsorb MB from the wastewater as shown in Figure 6. The batch adsorption experiments are carried out by taking SCSW and ABC as an adsorbent with varying reaction times and maintaining the reaction temperature, dye concentration, adsorbent dose, pH, and rpm constant at 50 °C, 20 mg/L, 5 g/L, 5.5, and 125 rpm, respectively. It is apparent from Figure 6 that adsorption is intensified for ABC compared to SCSW due to its improved porosity and surface area, less dissolved carbon content, presence of metal oxides, and hydrophobic nature as indicated by the BET surface area, ultimate, XRF, and SEM analysis as discussed in the previous section. Figure 6 shows that the adsorption capacity and dye removal curves are increased linearly up to 40 min, reaching their equilibrium value and becoming asymptotic after 40 min. The equilibrium value signifies that the active sites present onto the surface of adsorbent (SCSW/ABC) are fully engaged by MB molecules and no further adsorption may happen. Quasi-static equilibrium is attained in 120 min for both SCSW and ABC. However, ABC shows higher adsorption capacity and dye removal as 3.8 ± 4% mg/g and 99 ± 4%, respectively, in comparison with SCSW, i.e. 3.5 ± 4% mg/g and 89 ± 4% in 120 min reaction time. As it is already explained in Section 3.1 that the SCSW surface is negatively charged above 6.2 pH, the adsorption of the MB dye (basic dye) onto the surface would be favorable. Hence it can be concluded from adsorption experiments that SCSW

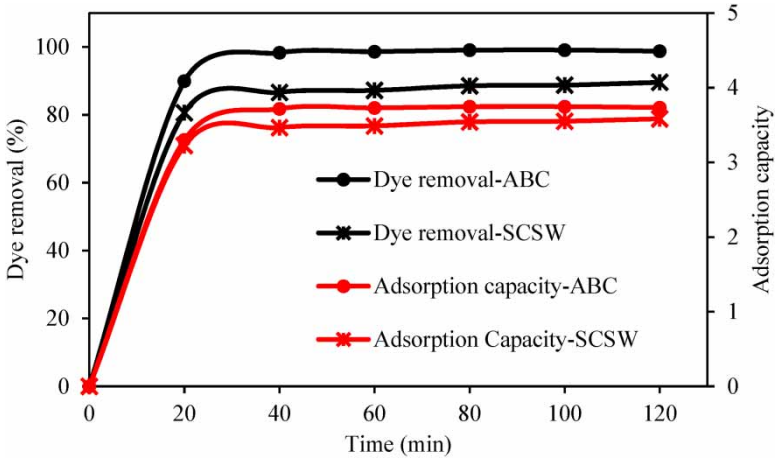

Figure 6 | Adsorption of MB dye-containing wastewater using SCSW and ABC (temp. = 50 °C, dye conc. = 20 mg/L, adsorbent dose = 5 g/L, pH = 5.5, and rpm = 125).

possesses the favorable adsorbent characteristics to treat MB dye-bearing wastewater which are further enhanced by converting SCSW into ABC. Operating parameters such as pH, adsorbent dose, initial dye concentration, and reaction temperature critically affect the adsorption of organic pollutant from water. Hence the effect of these parameters on the adsorption of MB using ABC is carried out and presented in the following sections.

3.5. Influence of parameters

The effect of pH on the adsorption of MB using ABC is studied by varying the pH of the dye solution from acidic to basic range as presented in Figure 7(a), whereas the temperature, ABC dose, and dye concentration are kept fixed at 30 °C, 5 g/L, and 20 ppm, respectively. It depicts that dye removal as well as adsorption capacity is increased at higher pH of the dye solution; hence, maximum dye removal was attained at pH equal to 11. This behavior of pH variation can be explained with the help of pH_{zpc} of ABC, i.e. 10 and pKa value of MB dye, i.e. 5.8 (Gadelha *et al.* 2023). The ABC surface is positively charged while MB is negatively charged below pH 5.8 that results in adsorption of MB onto the ABC surface mainly driven by the electrostatic attraction. In the pH range 5.8–10, adsorption is primarily driven by Van der Waals forces, however at pH > 10, electrostatic interaction once again takes over (Gadelha *et al.* 2023). The ABC surface is negatively charged due to protonation above pH 10 which enhances the adsorption of cationic MB dye as shown in Figure 7(a). Moreover, when the pH exceeds the point-of-zero charge pH_{zpc} a negative charge develops at the interface between MB and the adsorbent in addition to the strong acid sites. This enhances the attraction between MB dye and ABC, facilitating increased dye adsorption onto ABC.

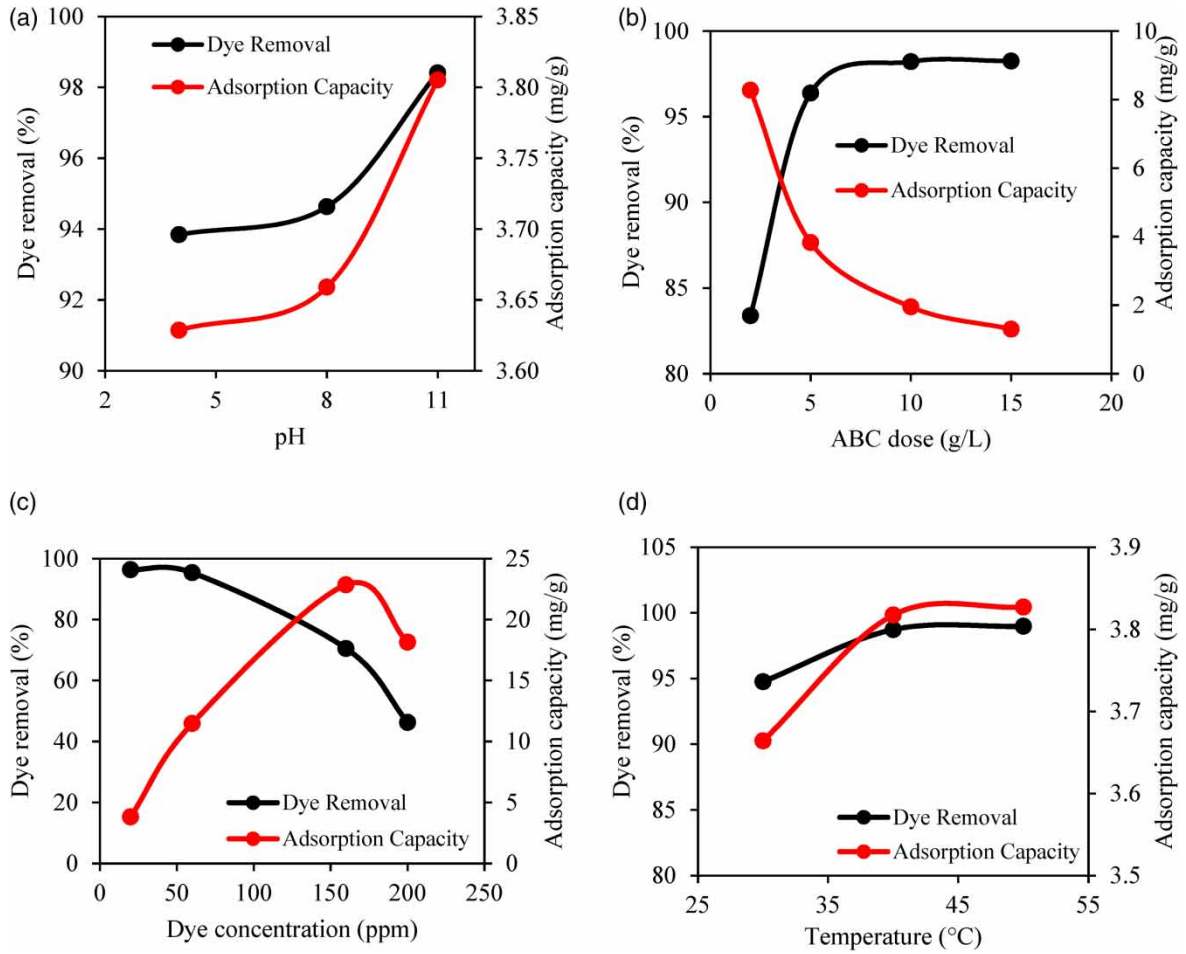

Figure 7 | Effect of (a) pH, (b) ABC–SCSW dose, (c) dye concentration, and (d) temperature on the MB dye adsorption.

Figure 7(b) depicts the influence of ABC doses on the dye removal and adsorption capacity by varying dose from 2 to 15 g/L while temperature, pH, and dye concentration are fixed at 30 °C, 6.5 (natural pH), and 20 ppm, respectively. It is visible that the dye removal is enhanced with the ABC till 5 g/L and then becomes

constant till 15 g/L. Hence, the optimal dye removal obtained at 5 g/L is 97% and further increase in ABC mass does not affect the removal due to unavailability of enough MB binding sites since dye concentration is constant (Wakejo *et al.* 2023). On the other hand, the adsorption capacity of ABC is decreased continuously with the rise in ABC dose from 2 to 15 g/L and higher adsorption capacity is found at the lowest adsorbent dose, i.e. 2 g/L due to an increase in the ratio of dye to adsorbent molecules (Zubair *et al.* 2020). When adsorbent dose is increased keeping dye concentration constant, the availability of binding sites per dye molecule increases which results in lower adsorption capacity (Zubair *et al.* 2020). It indicates that most of the adsorbent sites are not participating in adsorption and remain idle in the solution which can be used if the dye concentration is increased.

The initial dye concentration is likely one of the most significant parameters affecting the adsorption process since it directly affects the dye removal and adsorption capacity as mentioned in Equations (3) and (4). The influence of dye concentration on the adsorption of MB is studied by varying the concentration from 20 to 200 ppm and is shown in Figure 6(c). Other parameters such as pH, ABC dose, and temperature are kept fixed at 6.5 (natural pH), 5 g/L, and 30 °C. The dye removal is maximum at low dye concentration, i.e. 20 ppm and keeps on decreasing with increasing dye concentration. Since the ABC dose is constant for all the variation in dye concentration, the number of dye molecules available to bind with the active sites of ABC increases with the increase in dye concentration and compete for active sites (Wakejo *et al.* 2023). Hence it can be perceived that at 20 ppm, enough dye molecules are available to fully bind to the active sites present at 5 g/L of ABC dose and results in highest dye removal as shown in Figure 7(b). In contrast to dye removal, adsorption capacity is increased with initial dye concentration till 160 ppm due to a decrease in mass transfer resistance (Wakejo *et al.* 2023); however, further increase in dye concentration to 200 ppm decreases the adsorption. This could be due to the rise in equilibrium adsorption capacity with increasing initial dye concentration (Wakejo *et al.* 2023).

The temperature at which the adsorption reaction occurs is a crucial parameter, as it can shift the nature of the reaction from endothermic to exothermic and vice versa, thereby affecting the reaction's outcome. To study the influence of reaction temperature on the adsorption of MB on the ABC surface, experiments are performed by varying temperatures from 30 to 50 °C and keeping pH, ABC dose, and dye concentration fixed at 6.5, 5 g/L, and 20 ppm, respectively. Figure 7(d) shows that dye removal as well as adsorption capacity increases with temperature due to enhancement in reaction rate and maximum value is attained at 50 °C (Rápó & Tonk 2021). It also indicates that the adsorption of MB onto the ABC surface is an endothermic adsorption because the activation of the adsorbent surface takes place at higher temperature, facilitating the mobility of large dye ions toward the active sites (Rápó & Tonk 2021).

Based on parametric studies, the optimal conditions to maximize the MB dye removal and adsorption capacity are selected and experimental runs are performed. The optimal conditions for dye removal and adsorption capacity are estimated as 10 pH, 10 g/L of the ABC dose, 20 ppm and 50 °C and 10 pH, 2 g/L of the ABC dose, 160 ppm, and 50 °C, respectively, which results in 99.6% dye removal and 66.5 mg/g of adsorption capacity. Therefore, it can be inferred that biochar derived from SCSW possesses outstanding adsorbent properties, making it a viable option for efficient implementation in wastewater treatment processes. A comparison study, as illustrated in Table 3, reveals that ABC demonstrates superior adsorption capabilities compared to alternate biosorbents for the adsorption of the MB dye. However, in case of pollutants other than MB, MCM-48 and Co/MCM-41 exhibit the highest adsorption capacity for 4-nitroaniline and sulfur, respectively, using a fixed bed adsorption column.

Table 3 | Comparison among other adsorbents in terms of adsorption capacity

Biosorbent	Organic pollutant	Maximum adsorption capacity (mg/g)	References
Sewage sludge biochar	MB	24	Fan *et al.* (2017)
HNO_3-activated biochar	MB	37.18	Wang *et al.* (2018)
Rice husk	MB	40.5	Vadivelan & Vasanth Kumar (2005)
Corn husk	MB	41.55	Paşka *et al.* (2014)
ABC	MB	66.5	This work
MCM-48	4-nitroaniline	90	Ali *et al.* (2023)
Co/MCM-41	Sulfur	1,310 (fixed bed column)	Khadim *et al.* (2022)

3.6. Adsorption kinetics

Adsorption kinetics plays a pivotal role in validating experimental findings and discerning the rate-controlling phase within the adsorption mechanism in the context of the MB-SCSW and MB-ABC adsorption systems. Pseudo-first-order, pseudo-second-order, and intra-particle diffusion models are used in this adsorption system to understand adsorption kinetics. Table 4 and Figures 8(a) and 8(b) reveal that the experimental Q_e values for SCSW and ABC closely align with the calculated Q_e values for pseudo-first-order and pseudo-second-order kinetics, respectively, as indicated by the coefficient of determination ($R^2 = 0.99$) also. Conversely, the intraparticle diffusion model demonstrates inadequacy for the MB-SCSW and MB-MBC adsorption systems, as evidenced by its lower $R^2 = 0.7$ value. It is evident that for both systems, the adsorption mechanism primarily involves the chemisorption of MB dye molecules onto the surfaces of SCSW and ABC (Ali *et al.* 2022a).

Table 4 | Kinetic adsorption data of SCSW and ABC

Kinetic models	SCSW	ABC
Q_e (mg/g) (experimental) @ $T = 50$ °C, $C_o = 20$ mg/L, dose = 0.5 g, pH = 5.5, rpm = 125	**3.5 ± 4%**	**3.8 ± 4%**
Pseudo first-order kinetic model, $Q_t = Q_e(1 - e^{-k_1 t})$, Q_t is the adsorption capacity at time t.		
Q_e (mg/g) (Calculated)	3.5334	3.74887
k_1 (1/min) – rate constant	0.1206	0.09926
R^2	0.9994	0.9998
Pseudo second-order kinetic model, $Q_t = \frac{Q_e^2 k_2 t}{1 + Q_e k_2 t}$		
Q_e (mg/g) (Calculated)	3.6553	3.92423
k_2 (g/mg min) – rate constant	0.1054	0.06679
R^2	0.9998	0.9968
Intraparticle diffusion kinetic model, $Q_t = K_{diff} t^{0.5} + C$		
K_{diff} (mg/g.min$^{0.5}$) – rate coefficient of diffusion	0.30054	0.32033
C – boundary layer thickness	0.8993	0.91119
R^2	0.7335	0.7478

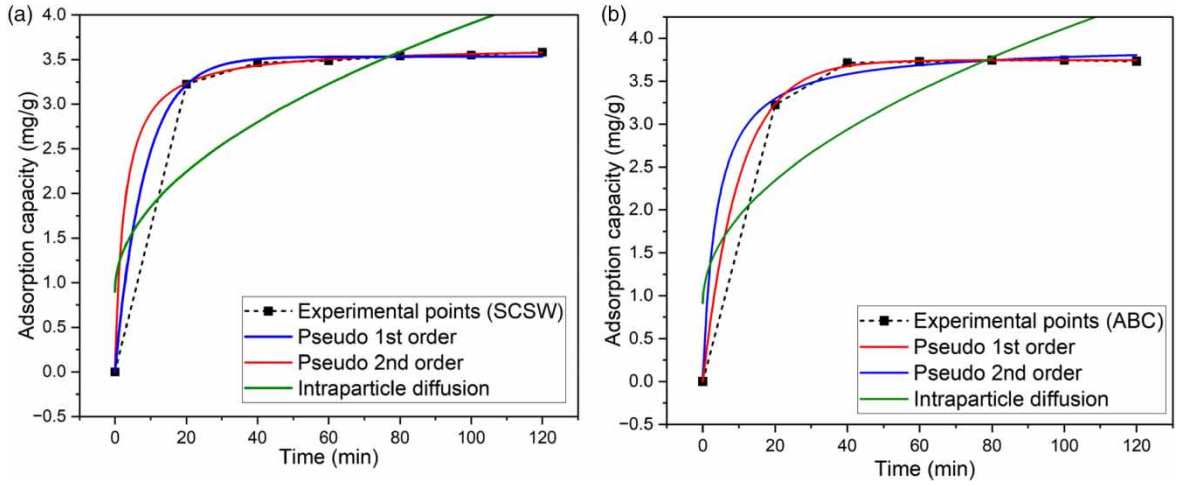

Figure 8 | Kinetic analysis of (a) MB-SCSW and (b) MB-ABC adsorption systems.

4. CONCLUSION

This study investigates the strategies to utilize SCSW from the essential oil industry for two purposes: bio-oil production and the treatment of wastewater through adsorption. TGA and FTIR study reveals the presence of biopolymer functional groups (cellulose, hemicellulose, lignin), suggesting its suitability for bio-oil production. Additionally, TPD and pH_{zpc} analysis confirm strong acidic surface sites on the SCSW sample, ideal for

adsorbing basic dyes. In light of the aforementioned details, the pyrolysis of SCSW at 500 °C results in the production of a significant quantity of bio-oil (45 wt%) and biochar (25wt%). Bio-oil comprises of carboxylic acids, phenols, aromatic hydrocarbons, and aliphatic hydrocarbons, whereas biochar (ABC) exhibits a significant augmentation in surface area and roughness, presenting robust adsorption sites in comparison to SCSW. Upon comparing the efficacy of ABC and SCSW for MB dye adsorption, ABC emerges as the superior adsorbent, achieving a maximum dye removal of 99.6% and an adsorption capacity of 66.5 mg/g under optimal conditions. These conditions include 10 pH, 10 g/L of the dose, 20 ppm of dye concentration, and 50 °C for dye removal and 10 pH, 2 g/L of the ABC dose, 60 ppm of dye concentration, and 50 °C for adsorption capacity. Kinetic study reveals that SCSW and ABC both follow pseudo-first-order kinetic. Hence, it can be concluded that SCSW not only demonstrates remarkable potential in wastewater treatment as an adsorbent but also emerges as an exceptional feedstock for bio-oil production. This two-fold utilization of SCSW represents a sustainable and circular approach, harnessing its full potential and contributing to a greener, more resource-efficient future.

ACKNOWLEDGEMENTS

The authors would like to thank Shiv Nadar (Institution of Eminence Deemed to be University) for providing experimental and financial support. The authors would also like to thank Head of the Department, Department of Chemical Engineering, IIT Roorkee for the characterizations (BET, NH_3-TPD).

FUNDING

This research did not receive any specific grant from funding agencies in the public, commercial, or not-for-profit sectors.

DATA AVAILABILITY STATEMENT

Data cannot be made publicly available; readers should contact the corresponding author for details.

CONFLICT OF INTEREST

The authors declare there is no conflict.

REFERENCES

Abdel-Rahman, L. H., Abu-Dief, A. M., Abd-El Sayed, M. A. & Zikry, M. M. 2016 Nano sized *moringa oleifera* an effective strategy for Pb(II) ions removal from aqueous solution. *Chemistry and Materials Research* **8**(4), 8–22.

Abu-Dief, A. M., Abdel-Rahman, L. H., Abd–ElSayed, M. A. & Zikry, M. M. 2021a Green synthesis of silver nanoparticles using *Delonix regia* extract, characterization and its application as adsorbent for removal of Cu (II) ions from aqueous solution. *Asian Journal of Applied Chemistry Research* **9**(1), 1–15.

Abu-Dief, A. M., Essawy, A. A., Diab, A. K. & Mohamed, W. S. 2021b Facile synthesis and characterization of novel Gd_2O_3–CdO binary mixed oxide nanocomposites of highly photocatalytic activity for wastewater remediation under solar illumination. *Journal of Physics and Chemistry of Solids* **148**, 109666. https://doi.org/10.1016/j.jpcs.2020.109666.

Alahmadi, M., Alsaedi, W. H., Mohamed, W. S., Hassan, H. M. A., Ezzeldien, M. & Abu-Dief, A. M. 2023 Development of Bi_2O_3/$MoSe_2$ mixed nanostructures for photocatalytic degradation of methylene blue dye. *Journal of Taibah University for Science* **17**(1). https://doi.org/10.1080/16583655.2022.2161333.

Ali, N. S., Jabbar, N. M., Alardhi, S. M., Majdi, H. S. & Albayati, T. M. 2022a Adsorption of methyl violet dye onto a prepared bio-adsorbent from date seeds: Isotherm, kinetics, and thermodynamic studies. *Heliyon* **8**(8), e10276. https://doi.org/10.1016/j.heliyon.2022.e10276.

Ali, N. S., Kalash, K. R., Ahmed, A. N. & Albayati, T. M. 2022b Performance of a solar photocatalysis reactor as pretreatment for wastewater via UV, UV/TiO_2, and UV/H_2O_2 to control membrane fouling. *Scientific Reports* **12**(1), 1–10. https://doi.org/10.1038/s41598-022-20984-0.

Ali, N. S., Harharah, H. N., Salih, I. K., Cata Saady, N. M., Zendehboudi, S. & Albayati, T. M. 2023 Applying MCM-48 mesoporous material, equilibrium, isotherm, and mechanism for the effective adsorption of 4-nitroaniline from wastewater. *Scientific Reports* **13**(1), 1–14.

Alismaeel, Z. T., Al-Jadir, T. M., Albayati, T. M., Abbas, A. S. & Doyle, A. M. 2022 Modification of FAU zeolite as an active heterogeneous catalyst for biodiesel production and theoretical considerations for kinetic modeling. *Advanced Powder Technology* **33**(7), 103646. https://doi.org/10.1016/j.apt.2022.103646.

Al-Jaaf, H. J., Ali, N. S., Alardhi, S. M. & Albayati, T. M. 2022 Implementing eggplant peels as an efficient bio-adsorbent for treatment of oily domestic wastewater. *Desalination and Water Treatment* **245**, 226–237.

Almendros, A. I., Martín-Lara, M. A., Ronda, A., Pérez, A., Blázquez, G. & Calero, M. 2015 Physico-chemical characterization of pine cone shell and its use as biosorbent and fuel. *Bioresource Technology* **196**, 406–412.

Alzaid, M., Mohamed, W. S., Alanazi, R., Alsohaimi, I. H., Hassan, H. M. A., Hadia, N. M. A., Ezzeldien, M., El-Aassar, M. R. & Abu-Dief, A. M. 2023 Novel (Y_2O_3) x (CdO) 1-x binary mixed oxide nanocomposites: Facile synthesis, characterization, and photocatalysis enhancement. *Journal of Materials Research and Technology* **23**, 2454–2466. https://doi.org/10.1016/j.jmrt.2023.01.105.

Cychosz, K. A. & Thommes, M. 2018 Progress in the physisorption characterization of nanoporous gas storage materials. *Engineering* **4**(4), 559–566. https://doi.org/10.1016/j.eng.2018.06.001.

Das, P. & Debnath, A. 2021 Reactive orange 12 dye adsorption onto magnetically separable $CaFe_2O_4$ nanoparticles synthesized by simple chemical route: Kinetic, isotherm and neural network modeling. *Water Practice and Technology* **16**(4), 1141–1158.

dos Santos, K. J. L., dos Santos, G. E. d. S., de Sá, Í. M. G. L., Ide, A. H., Duarte, J. L. d. S., de Carvalho, S. H. V., Soletti, J. I. & Meili, L. 2019 *Wodyetia bifurcata* biochar for methylene blue removal from aqueous matrix. *Bioresource Technology* **293**, 122093.

Fan, S., Wang, Y., Wang, Z., Tang, J., Tang, J. & Li, X. 2017 Removal of methylene blue from aqueous solution by sewage sludge-derived biochar: Adsorption kinetics, equilibrium, thermodynamics and mechanism. *Journal of Environmental Chemical Engineering* **5**(1), 601–611.

Gadelha, A. J. F., da Rocha, C. O., do Nascimento, M. R., Rocha, L. P., de Sousa, D. A. & da Cunha, B. V. 2023 Study of malachite green dye biosorption on acerola (*Malpighia emarginata*) seeds for the treatment of coloured wastewater: Kinetics, equilibrium, and experimental design. *Water Practice & Technology* **18**(6), 1465–1478.

Get News. 2022 *Essential Oils Market is Predicted to Witness A CAGR of 7.4% in Terms of Revenue by 2028, Driven by Increasing Inclination of People Towards Aromatherapy | Grand View Research, Inc. Digital Journal*. Available from: https://www.digitaljournal.com/pr/essential-oils-market-is-predicted-to-witness-a-cagr-of-7-4-in-terms-of-revenue-by-2028-driven-by-increasing-inclination-of-people-towards-aromatherapy-grand-view-research-inc.

Hemmann, F., Jaeger, C. & Kemnitz, E. 2014 Comparison of acidic site quantification methods for a series of nanoscopic aluminum hydroxide fluorides. *RSC Advances* **4**(100), 56900–56909. http://dx.doi.org/10.1039/C4RA09477H.

Khadim, A. T., Albayati, T. M. & Cata Saady, N. M. 2022 Removal of sulfur compounds from real diesel fuel employing the encapsulated mesoporous material adsorbent Co/MCM-41 in a fixed-bed column. *Microporous and Mesoporous Materials* **341**, 112020. https://doi.org/10.1016/j.micromeso.2022.112020.

Kumar, R. & Ahmad, R. 2011 Biosorption of hazardous crystal violet dye from aqueous solution onto treated ginger waste (TGW). *Desalination* **265**(1–3), 112–118.

Kumari, P. & Mohanty, B. 2020 Comparison of HZSM-5 catalyzed and non-catalyzed bio-oil produced using fast pyrolysis from pine needles. *Biomass and Bioenergy* **139**, 105641. https://doi.org/10.1016/j.biombioe.2020.105641.

Li, C., Zhang, J., Han, J. & Yao, B. 2021 A numerical solution to the effects of surface roughness on water–coal contact angle. *Scientific Reports* **11**(1), 1–12. https://doi.org/10.1038/s41598-020-80729-9.

Li, H., Li, T., Shi, W., Tian, Y., Liu, J. & Qin, X. 2022 Dye adsorption properties of poly(p-phenylene terephthalamide)-embedded hollow fiber composite membranes. *Reactive and Functional Polymers* **170**, 105135. https://doi.org/10.1016/j.reactfunctpolym.2021.105135.

Mohamed, W. S. & Abu-Dief, A. M. 2018 Synthesis, characterization and photocatalysis enhancement of Eu_2O_3-ZnO mixed oxide nanoparticles. *Journal of Physics and Chemistry of Solids* **116**, 375–385. https://doi.org/10.1016/j.jpcs.2018.02.008.

Mohsen Alardhi, S., Alrubaye, J. M. & Albayati, T. M. 2020 Removal of methyl green dye from simulated waste water using hollow fiber ultrafiltration membrane. *IOP Conference Series: Materials Science and Engineering* **928**(5), 1–13.

Mosoarca, G., Vancea, C., Popa, S., Gheju, M. & Boran, S. 2020 *Syringa vulgaris* leaves powder a novel low-cost adsorbent for methylene blue removal: Isotherms, kinetics, thermodynamic and optimization by Taguchi method. *Scientific Reports* **10**(1), 1–9. https://doi.org/10.1038/s41598-020-74819-x.

Omorogie, M. O., Babalola, J. O., Unuabonah, E. I., Song, W. & Gong, J. R. 2016 Efficient chromium abstraction from aqueous solution using a low-cost biosorbent: *Nauclea diderrichii* seed biomass waste. *Journal of Saudi Chemical Society* **20**(1), 49–57.

Paşka, O. M., Pəcurariu, C. & Muntean, S. G. 2014 Kinetic and thermodynamic studies on methylene blue biosorption using corn-husk. *RSC Advances* **4**(107), 62621–62630.

Rápó, E. & Tonk, S. 2021 Factors affecting synthetic dye adsorption; desorption studies: A review of results from the last five years (2017–2021). *Molecules* **26**(17), 1–31.

Saikia, N. & Bardalai, M. 2018 Thermal analysis and kinetic parameters determination of biomass using differential thermal gravimetric analysis in N_2 atmosphere. *Materials Today: Proceedings* **5**(1), 2146–2156. https://doi.org/10.1016/j.matpr.2017.09.212.

Santos, J., Ouadi, M., Jahangiri, H. & Hornung, A. 2019 Integrated intermediate catalytic pyrolysis of wheat husk. *Food and Bioproducts Processing* **114**, 23–30. https://doi.org/10.1016/j.fbp.2018.11.001.

Sieniawska, E., Swiątek, L., Rajtar, B., Koziol, E., Polz-Dacewicz, M. & Skalicka-Wozniak, K. 2016 Carrot seed essential oil – source of carotol and cytotoxicity study. *Industrial Crops and Products* **92**, 109–115.

Singh, D. & Yadav, S. 2019 Evaluation of the physico-chemical development of kitchen food wastes through torrefaction – a biodiversity case study. *Biomass Conversion and Biorefinery* **11**, 1353–1362.

Sowbhagya, H. B. 2019 Value-added processing of by-products from spice industry. *Food Quality and Safety* **3**(2), 73–80.

Vadivelan, V. & Vasanth Kumar, K. 2005 Equilibrium, kinetics, mechanism, and process design for the sorption of methylene blue onto rice husk. *Journal of Colloid and Interface Science* **286**(1), 90–100.

Wakejo, W. K., Meshesha, B. T., Kang, J. W. & Demesa, A. G. 2023 Bamboo sawdust-derived high surface area activated carbon for remarkable removal of paracetamol from aqueous solution: Sorption kinetics, isotherm, thermodynamics, and regeneration studies. *Water Practice & Technology* **18**(6), 1366–1388.

Wang, S., Guo, Z., Cai, Q. & Guo, L. 2012 Catalytic conversion of carboxylic acids in bio-oil for liquid hydrocarbons production. *Biomass and Bioenergy* **45**, 138–143. http://dx.doi.org/10.1016/j.biombioe.2012.05.023.

Wang, Y., Zhang, Y., Li, S., Zhong, W. & Wei, W. 2018 Enhanced methylene blue adsorption onto activated reed-derived biochar by tannic acid. *Journal of Molecular Liquids* **268**, 658–666.

Wang, S., Li, X. & Zhu, Y. 2023 Comparison of the adsorption capacity and mechanisms of mixed heavy metals in wastewater by sheep manure biochar and *Robinia pseudoacacia* biochar. *Water Science & Technology* **87**(12), 3083–3094.

Yin, F., Zhuang, Q., Chang, T., Zhang, C., Sun, H., Sun, Q., Wang, C. & Li, L. 2021 Study on pyrolysis characteristics and kinetics of mixed plastic waste. *Journal of Material Cycles and Waste Management* **23**(5), 1984–1994. https://doi.org/10.1007/s10163-021-01271-y.

Zubair, M., Mu'azu, N. D., Jarrah, N., Blaisi, N. I., Aziz, H. A. & Al-Harthi, M. A. 2020 Adsorption behavior and mechanism of methylene blue, crystal violet, eriochrome black T, and methyl orange dyes onto biochar-derived date palm fronds waste produced at different pyrolysis conditions. *Water Air & Soil Pollution* **231–240**, 1–19. Available from: https://www.franceagrimer.fr/fam/content/download/67094/document/Marche_olive_2019_2020.pdf?version=1.

First received 18 July 2023; accepted in revised form 15 September 2023. Available online 5 October 2023